8-5-2009

Complex Dielectric Permittivity Measurements from Ground-Penetrating Radar Data to Estimate Snow Liquid Water Content in the Pendular Regime

John H. Bradford
Boise State University

Joel T. Harper
University of Montana

Joel Brown
Boise State University

 DOI: 10.1029/2008WR007341

Complex dielectric permittivity measurements from ground-penetrating radar data to estimate snow liquid water content in the pendular regime

John H. Bradford,[1] Joel T. Harper,[2] and Joel Brown[1]

Received 5 August 2008; revised 27 April 2009; accepted 28 May 2009; published 5 August 2009.

[1] Monitoring the snow water equivalent (SWE) is critical to effective management of water resources in many parts of the world that depend on the mountain snowpack for water storage. There are currently no methods to remotely sense SWE with accuracy over large lateral distances in the steep and often forested terrain of mountain basins. Previous studies have shown that measurements of ground-penetrating radar (GPR) velocity can provide accurate estimates of SWE in dry snow. Introduction of liquid water into the snowpack results in a three-phase system that cannot be accurately characterized with GPR velocity alone. We show that measuring the frequency-dependent GPR signal attenuation and velocity provides a direct estimate of the complex dielectric permittivity. Because the imaginary component is a function only of liquid water content, we can utilize both the real and imaginary components of the permittivity to estimate liquid water content, snow density, and SWE using existing empirical relationships that are valid in the pendular regime. We tested this new method at two field sites and found that the estimates were accurate to within 12% of gravimetric methods in both a moist and a dry snowpack. GPR has the potential to provide SWE estimates across large lateral distances over a broad range of snow conditions.

Citation: Bradford, J. H., J. T. Harper, and J. Brown (2009), Complex dielectric permittivity measurements from ground-penetrating radar data to estimate snow liquid water content in the pendular regime, *Water Resour. Res.*, *45*, W08403, doi:10.1029/2008WR007341.

1. Introduction

[2] Many semiarid parts of the world depend heavily on mountain snow packs for water supply and storage. For example, estimates suggest that in the western U.S., flow in rivers derived directly from snowmelt is on the order of 40–75% [*Cayane*, 1996; *Serreze et al.*, 1999]. Agricultural, recreational, and environmental demands for this water are greatest during the west's characteristic warm and dry summers. In many mountain basins, snow rather than built storage, is the primary reservoir for holding winter precipitation for later release in summer [*Hamlet et al.*, 2005]. During episodes of prolonged drought the reliance on snow storage is intensified. If the current trends at sampled locations are extrapolated to the landscape and projected into the future, significant reductions in water availability are predicted [*Hamlet et al.*, 2005; *Stewart et al.*, 2004]. The time frame for far-reaching impacts is on the order of years to decades, not centuries.

[3] Perhaps the most fundamental problem in evaluating snow water resources is the lack of adequate methods for measuring Snow Water Equivalent (SWE) at the watershed scale. Topography, vegetation, and microclimatic effects cause large variability in SWE; in shallow snowcovers it can vary by more than 50% within 10 meters, and standard deviations of 60–180% relative to the basin mean have been measured within alpine watersheds [*Elder et al.*, 1991]. Remote sensing methods can determine snow coverage, but do not provide adequate measure of snow depth or water content in the steep and forested terrain of western U.S. mountain basins. Consequently, in the western U.S. point measurements from only a few automatic snow pillows (SNOTEL) or monthly manual measurements at select locations (Snow Course) are available for estimating SWE across an entire basin. These data are integrated with multidecadal stream flow records utilizing empirical relationships to predict total basin discharge. Since this approach is based on historical averages, it may break down with increased climactic variability, and this problem necessitates high-resolution SWE measurements for accurate water resource characterization. Traditional point measurements are expensive and time consuming and may never fully capture important lateral heterogeneity in the snowpack [*Bales et al.*, 2006].

[4] Snow that contains liquid water can be broken into two categories with distinctly different physical properties: (1) the pendular regime where at low wetness, isolated water bodies exist in the pore volume, and (2) the funicular regime, where with increased wetness, the water droplets join to form continuous liquid paths through the connected pore space. The pendular-funicular transition occurs between

[1] Center for Geophysical Investigation of the Shallow Subsurface, Boise State University, Boise, Idaho, USA.
[2] Department of Geosciences, University of Montana, Missoula, Montana, USA.

0043-1397/09/2008WR007341$09.00

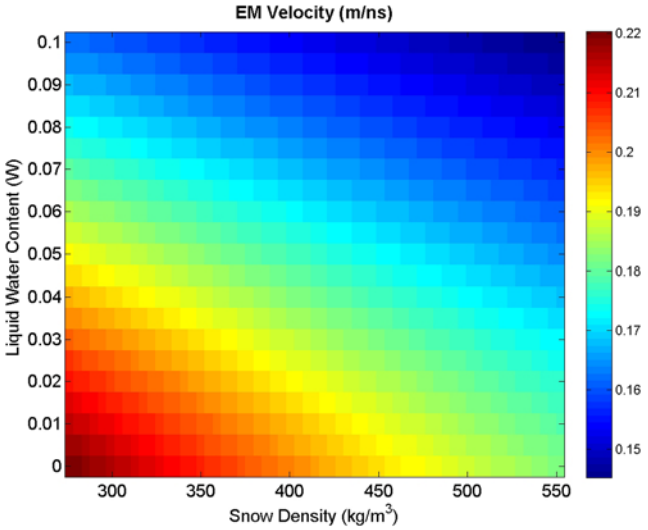

Figure 1. Plot showing the electromagnetic wave velocity as a function of snow density and wetness computed using equations (3)–(5).

~10–15% saturation of the pore volume [*Denoth*, 1980, 2003]. Snow is typically classified in the field according to its volumetric water content or wetness (W). Categories include dry (W = 0.00), moist (W = 0–0.03), wet (W = 0.03–0.08), very wet (W = 0.08–0.15), and slush (W > 0.15) [*Green et al.*, 2004]. Moist and wet snow fall into the pendular regime whereas very wet snow and slush are above the pendular-funicular transition. Field classification is determined qualitatively by such criteria as clumping or the amount of water drainage under hand squeezing.

[5] Ground-penetrating radar (GPR) is a tool that can provide laterally continuous measurements of snow properties. Here we present a new method for estimating W in the pendular regime using frequency-dependent attenuation analysis of ground-penetrating radar (GPR) data, and utilize this new method to improve SWE estimates. Using numerical examples, we examine the potential for pitfalls related to fine-scale snow stratigraphy and ice layers. Finally, we test the method on two field data sets; the first was acquired over a cold, dry snowpack and the second was acquired over a moist, early spring snowpack.

2. Measuring SWE Using GPR

2.1. Review of GPR Signal Propagation

[6] In GPR studies, the transmitting antenna generates a broadband electromagnetic signal that then propagates through the subsurface and is reflected at boundaries separating materials with differing electric properties (dielectric permittivity, ε^*, magnetic permeability, μ^*, and electric conductivity, σ^*). The reflected wavefield is recorded with the receiving antenna and used to produce a reflector map that is an image of electric impedance contrasts in the subsurface. Impedance contrasts are primarily controlled by the dielectric permittivity in GPR studies. A significant impedance contrast typically occurs at the snow/ground interface and produces an easily identifiable reflection. Additionally, reflections may occur at the air/snow interface if the GPR is suspended above the surface, or at internal boundaries in the snowpack which can be caused by changes in density, liquid water content, or sediment inclusion.

[7] In general, ε^*, μ^*, and σ^* are complex quantities (i.e., $\varepsilon^* = \varepsilon' + i\varepsilon''$). The solution to Maxwell's equations can be given as a function of real effective permittivity ($\varepsilon_e = \varepsilon' - \sigma''/\omega$), and real effective conductivity ($\sigma_e = \sigma_{dc} + \varepsilon''\omega$) where ω is the angular frequency of the signal. In GPR studies, it is generally assumed that $\sigma'' = 0$. Further, in snow the magnetic permeability is equal to the permeability of free space (μ_0) and $\sigma_{dc} \approx 0$. As shown by *Bradford* [2007], with these assumptions and the low loss approximation, the attenuation coefficient (α) and radar velocity (v) can be written as

$$\alpha \approx \sqrt{\frac{\mu_0}{\varepsilon'}}\frac{\varepsilon''}{2}\omega \tag{1}$$

$$v \approx \frac{1}{\sqrt{\varepsilon'\mu_0}}. \tag{2}$$

2.2. Petrophysical Relationships for SWE Estimation

[8] In dry snow, radar velocity is primarily a function of snow density [*Tiuri et al.*, 1984]. Several authors have demonstrated that with an estimate of radar velocity, either through multioffset measurements, or by calibration with measured snow depth, SWE of dry snow can be determined to within about 5–10% [*Ellerbruch and Boyne*, 1980; *Gubler and Hiller*, 1984; *Harper and Bradford*, 2003; *Marshall et al.*, 2005; A. P. Annan et al., GPR for snow pack water content, paper presented at GPR '94, The Fifth International Conference on Ground Penetrating Radar, Waterloo Center for Groundwater Research, Kitchener, Ontario, Canada, 1994]. There is a large permittivity contrast between ice and liquid water ($\varepsilon_W/\varepsilon_I \approx 29$) so that introduction of a small amount of water into the snowpack significantly alters the dielectric properties. In this case, radar velocity is a function of both snow density and liquid water content (Figure 1), and it is not possible to measure SWE on the basis of velocity alone. *Lundberg and Thunehed* [2000] discussed the effect of liquid water content in the context of calibrating GPR two-way traveltime measurements but also note the difficulty in obtaining reliable field measurements of liquid water for estimating calibration constants. Conversely, frequency-dependent signal attenuation, to a good approximation, is a function only of water content. For example, *Tiuri et al.* [1984] and *Sihvola and Tiuri* [1986] gave the following set of empirical equations that relate ε^* to liquid water content and snow density

$$\varepsilon'_d = \left(1 + 1.7\rho_d + 0.7\rho_d^2\right) \tag{3}$$

$$\varepsilon'_s = \left(0.10W + 0.80W^2\right)\varepsilon'_w + \varepsilon'_d \tag{4}$$

$$\varepsilon''_s = \left(0.10W + 0.80W^2\right)\varepsilon''_w \tag{5}$$

where W is snow wetness (by volume), ρ_d is the equivalent dry snow density in g/cm^3, and the subscripts w, s, and d

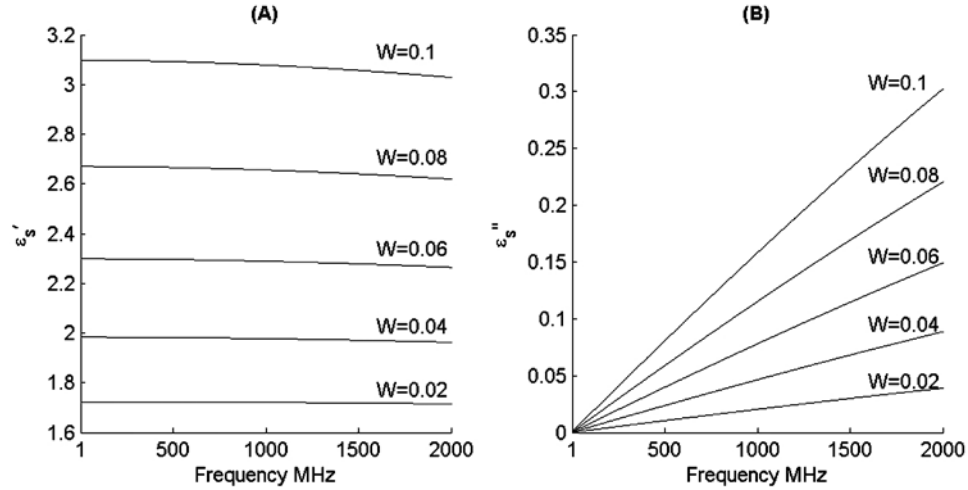

Figure 2. Real and imaginary permittivity as a function of frequency and wetness for snow with a density of 275 kg/m^3. The real permittivity is approximately independent of frequency, particularly below 1000 MHz, but increases rapidly with wetness. The imaginary permittivity depends strongly on frequency and wetness, therefore higher frequency radar is more sensitive to wetness. Note that we computed the complex permittivity of water using the dual Cole-Cole relaxation mechanism given by *Olhoeft* [1981].

indicate the properties of water, the snow being measured, and the equivalent dry snow properties respectively. Note that for equations (3)–(5), and throughout the remainder of this paper, subscripted permittivity is relative permittivity. Equations (3)–(5) are valid at 1 GHz for snow in the pendular regime ($W/\varphi < 10-15\%$: φ is porosity). It is still possible to utilize equations (3)–(5) for measurements made at other frequencies by noting that the loss tangent for water is approximately linear with frequency and the real part of the permittivity is approximately independent of frequency in the range from 1 MHz–2 GHz. This linearity means we may reduce the measured complex permittivity to the approximate value at 1 GHz simply by multiplying the measured value by 10^9/f, where f is the measurement frequency [*Tiuri et al.*, 1984]. In this study, we utilize the Finnish Snow Fork [*Sihvola and Tiuri*, 1986] for comparison to GPR measurements of liquid water content and snow density. This device measures the complex permittivity of snow and utilizes equations (3)–(5) to compute the snow properties. To establish a common basis for comparison we also utilize equations (3)–(5) in our analysis, but note that any appropriate model that relates liquid water content and snow density to complex dielectric permittivity may be substituted. *Lundberg and Thunehed* [2000] provided a review of several such models.

2.3. GPR Parameter Estimation

2.3.1. Velocity Analysis

[9] Using equations (1)–(5), quantitative estimates of radar attenuation and velocity provide a measure of the density, liquid water content, and SWE of snow. There are a variety of established methods we can use to measure radar velocity including moveout analysis of reflectors in common-midpoint (CMP) gathers [*Fisher et al.*, 1992; *Greaves et al.*, 1996; Annan et al., presented paper, 1994], moveout analysis of diffraction hyperbolas [e.g., *Bradford and Harper*, 2005], reflection tomography [e.g., *Bradford*, 2006; *Stork*, 1992], or point measurements of depth to the snow-ground interface, with a probe for example, followed by calibration with traveltime [e.g., *Marshall et al.*, 2005]. To measure attenuation, we apply the new method, described below, that utilizes the frequency dependence of signal attenuation.

2.3.2. Attenuation Analysis

[10] According to equation (1), a GPR signal propagating through snow undergoes frequency-dependent attenuation. Across the radar frequency band (10 MHz–1 GHz), ε' is approximately independent of frequency but depends strongly on W (Figure 2). Conversely, the attenuation is primarily a function of ε'' which increases rapidly with frequency and W (Figure 2). In dry snow $\varepsilon'' \approx 0$, and there is little intrinsic attenuation of the signal.

[11] The frequency dependence of ε''_s in snow with liquid water content follows the frequency dependence of ε''_w (equation (5)). *Turner and Siggins* [1994] demonstrated that the frequency-dependent attenuation of an electromagnetic wave propagating through water is, to a good approximation, linear with frequency over the bandwidth of a GPR signal. In this approximation, the attenuation coefficient can be written as

$$\alpha|_{\omega_1}^{\omega_2} = \alpha_0 + \frac{\sqrt{\mu_0 \varepsilon'}}{2Q^*}\omega \tag{6}$$

with the frequency-dependent component of attenuation characterized by the empirical constant Q^*. Here, ω_1 and ω_2 define the signal band, and α_0 includes the low-frequency terms that impact bulk radar attenuation. Note that Q^* is closely related to the loss tangent ($\tan\delta = \frac{\sigma_e}{\omega\varepsilon'}$). However, Q^* is purely empirical and utilized to make the linear approximation of equation (6).

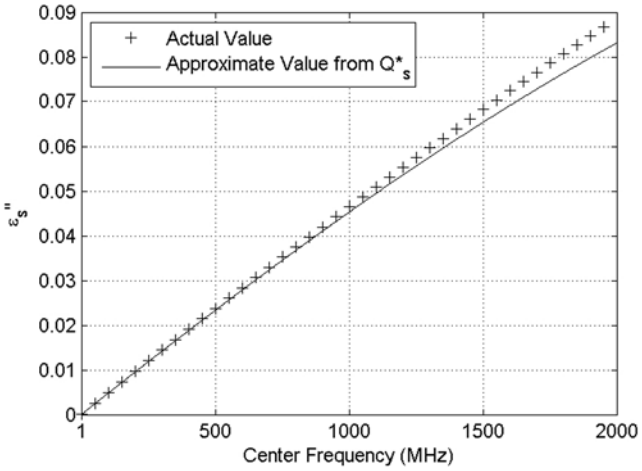

Figure 3. Imaginary component of water dielectric permittivity as a function of frequency. The plus shows the value computed using the dual Cole-Cole relaxation model given by *Olhoeft* [1981] and the solid line shows the approximation based on Q^* computed from a linear fit to the true attenuation coefficient curve over two octave bands. The approximate value is in good agreement with the exact value in the frequency range from 1 to 1500 MHz.

[12] *Bradford* [2007] derived the Taylor series expansion for the attenuation coefficient and showed that for water following a Debye relaxation mechanism, and frequency well below the relaxation frequency, the relationship between Q^* and the complex permittivity is given by

$$Q_w^* = \frac{\varepsilon_w'}{2\varepsilon_w''}. \tag{7}$$

Since ε_s'' and ε_s' are linear functions of ε_w'' and ε_w' in the GPR frequency band, we can compute Q_s^* using equation (7) with ε_s'' and ε_s'. Because the assumption of constant Q^* is valid only over the bandwidth of a typical GPR pulse, we take equation (7) to hold at the peak frequency of the pulse spectrum. Using a Cole-Cole relaxation model [*Olhoeft*, 1981] to compute the complex permittivity of water, equations (3)–(5) to compute the complex permittivity of wetted snow, and equation (6) to estimate Q^*, we find that the relationship given by equation (7) agrees with the true value for ε''_s to a good approximation across in the frequency range from 1–1500 MHz (Figure 3).

[13] As the signal propagates, high frequencies are attenuated more rapidly than low frequencies and the spectrum shifts toward lower frequencies. We can use this spectral shift to measure Q^* from field data using the frequency shift method [*Quan and Harris*, 1997]. The source waveform of many pulsed GPR systems approximates a Ricker wavelet. *Bradford* [2007] showed that the shift in peak frequency of Ricker wavelet spectrum is related to Q^* by

$$\frac{1}{Q^*} = \frac{2}{\pi t}\frac{\left(\omega_0^2 - \omega_t^2\right)}{\omega_0^2\omega_t}, \tag{8}$$

where $\omega_0 = 2\pi f_0$ is the spectral maximum at some reference time and $\omega_t = 2\pi f_t$ is the spectral maxima after propagation through the material for some time t. For other source spectra, it is necessary to derive expressions similar to equation (8) such as those for Guassian and boxcar spectra given by *Quan and Harris* [1997].

2.3.3. Practical Considerations

[14] Given equations (1)–(8), we utilize the following procedure to measure SWE using GPR.

[15] 1. Estimate radar velocity using a method such as those given in section 2.3.1: compute snow depth ($z = t^*v/2$) and ε' using equation (2).

[16] 2. Measure the peak frequency, f_0, of the reference wavelet and peak frequency, f_t, of the snow-ground reflection at time t: compute Q_s^*, and ε_s'' using equations (7) and (8).

[17] 3. Use equations (3)–(5) to estimate SWE given that SWE = $(\rho_d + W)z$, with density in g/cm^3.

[18] For attenuation analysis we identify the reflection from the base of the snow, then compute the Hilbert transform of the trace and find the local maxima of the envelope function within a time gate bounding the reflection. The instantaneous frequency at the peak of the envelope function provides a reliable estimate of the average frequency of the reflection [*Robertson and Nagomi*, 1984]. For a Ricker wavelet, the peak frequency is related to the mean frequency by $f_p = \frac{\bar{f}}{1.13}$.

[19] The reference frequency we choose significantly impacts our result, and errors can lead to misinterpretation. Choosing a set frequency, e.g., the manufacturer specified antenna frequency, is not effective in most cases; for a surface coupled system, antenna loading and variations in loading caused by surface heterogeneity alter the signal spectrum, and for either airborne or surface-coupled deployment system drift can cause variability in the source spectrum. We propose two methods for estimating a data driven variable reference frequency. For a surface-coupled system we can use the direct wave. For data acquired with the antennas at least one wavelength above the snow surface, we can use the reflection from the air/snow interface. In the field studies section below, we investigate both methods. Since the peak frequency of the signal changes as a function of propagation time, we use the mean of the reference and target reflector frequencies to scale the measurement to 1 GHz.

[20] One of the commonly recognized problems with Q^* analysis is that a number of factors can alter the reflected signal spectrum that are unrelated to the intrinsic attenuation (G. R. Olhoeft and D. E. Capron, Petrophysical causes of electromagnetic dispersion, paper presented at GPR '94, The Fifth International Conference on Ground Penetrating Radar, Waterloo Center for Groundwater Research, Kitchener, Ontario, Canada, 1994). *Bradford* [2007] showed that Q^* analysis can provide a reliable qualitative indicator of subsurface attenuation anomalies in sedimentary systems. Sedimentary systems are highly heterogeneous typically with multiple material types in multiple depositional configurations. Normally, neither the types of materials nor the configuration is fully constrained so that a quantitative relationship between GPR attenuation and subsurface properties is difficult or impossible. Here we argue that in the constrained snow system where there are often only three materials (assuming negligible impurities), water, ice, and air, we can make quantitative material property estimates. Below, we show that typical layering in snow will not significantly impact our measurement and

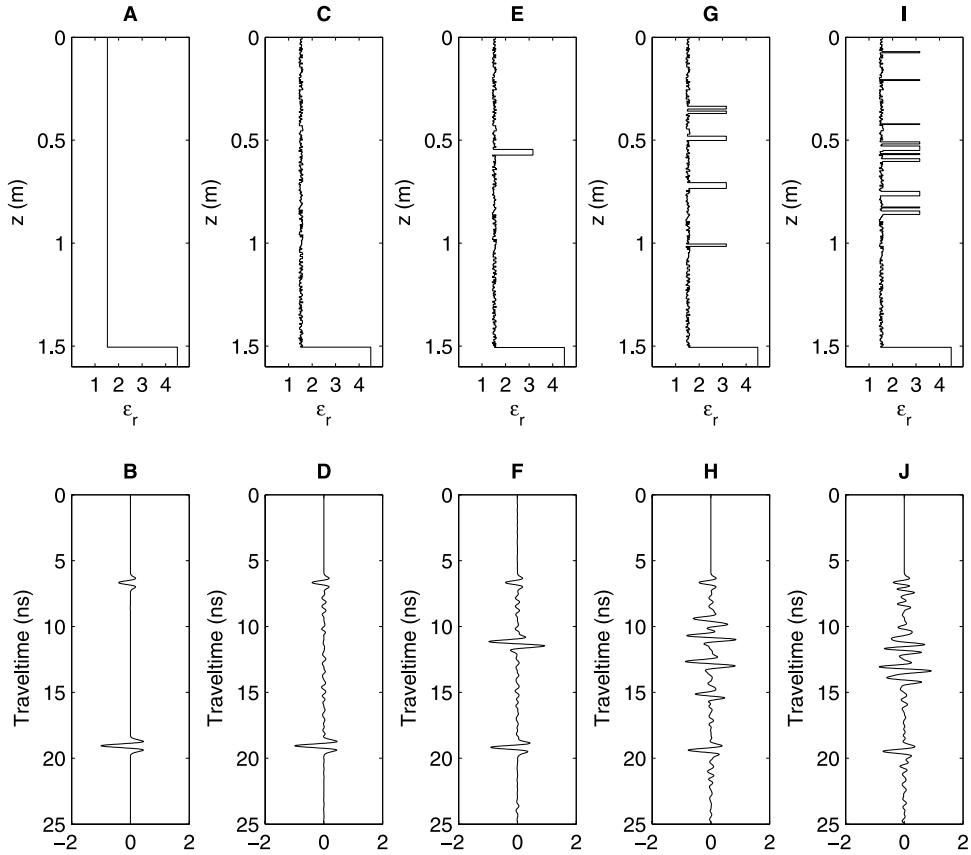

Figure 4. Dry snow relative permittivity models and simulated GPR traces for (A–B) homogeneous snow, (C–D) snow with 0.01 m layers and ±15% random density variations, (E–F) a single ice layer in model C, (G–H) five ice layers in model C, and (I–J) 10 ice layers in model C. In all cases, the average snow density is 275 kg/m^3.

illustrate the utility of the method through controlled field studies.

3. Vertical Heterogeneity in the Snow: A Numerical Example

[21] Up to this point, we have considered the snow a homogeneous medium. However, it is well known that as a signal propagates through a finely layered medium it undergoes scattering-induced, frequency-dependent attenuation that is comparable to intrinsic losses, and the two attenuation mechanisms cannot be differentiated [*Morlet et al.*, 1982]. Therefore the attenuation we measure in field data is a combination of intrinsic and scattering losses. Since snow is a finely layered medium it is important to understand the sensitivity of the attenuation measurement to conditions that might be observed in the field. We constructed a set of models to investigate the effect of scattering.

[22] For each model, we assume a 1.5 m thick dry snow pack with a background density of 275 kg/m^3. The first model is homogeneous snow. In the second model, we divide the snow into 0.01 m thick layers then randomly perturb the density of each layer by ±15%. Next we consider the effect of ice layers in the snow. The presence of thin ice layers is common, particularly in south facing or low-elevation snowpacks. Thin ice layers produce strong scattering and have significant potential to alter the observed signal spectrum. We construct three ice-layer models: the first has one layer, the second has five layers, and the third has 10 layers. The layers are randomly distributed and placed within the upper 1 m of our perturbed density model. The ice layer thickness varies randomly between 0 and 0.03 m. After inserting the ice layers, the bottom part of the snow model was truncated to maintain a constant 1.5 m snow thickness. In all cases, the snow is overlying a half space (ε_{so} = 4.5) which represents the underlying soil interface (Figure 4).

[23] To simulate GPR signal propagation, we use the reflectivity method. This method produces an exact, plane-wave solution to Maxwell's equations for a layered 1-D medium and is analogous to the reflectivity method for horizontal shear waves that is utilized in seismology [*Muller*, 1985]. The source is a 1200 MHz Ricker wavelet placed 1 m above the snow. The resulting data traces are plotted in Figure 4. The synthetic traces are qualitatively comparable to data we have recorded in the field under a variety of conditions. For each model, we compute the apparent water content utilizing the attenuation analysis procedure described in the previous section. The results of this analysis are summarized in Table 1.

[24] The frequency downshift for the perturbed snow model is 4 MHz giving an apparent volumetric water content (W_{app}) of 0.0003. This value is well below the measurement uncertainty we expect in field data and therefore we conclude that the effects of fine layering in typical snow may be neglected in most cases. For the one

Table 1. Results of Numerical Modeling Designed to Test the Sensitivity of the GPR Reflection Method to Layering in the Snow[a]

Model	Homogeneous	1 Ice Layer	5 Ice Layers	10 Ice Layers	Finely Layered Snow
$f_0 - f_t$	0	8 MHz	33 MHz	110 MHz	5 MHz
W_{app}	0.000	0.0004	0.0018	0.0059	0.0002

[a]In these models, no liquid water was present. The quantity $f_0 - f_t$ is the change in dominant frequency between the snow/air and snow/soil interface, and W_{app} is the apparent water content.

and five ice layer models, the downward shift is 1 MHz (W_{app} = 0.00008) and 21 MHz (W_{app} = 0.002) respectively. Again these values are negligible relative to uncertainty that is likely in field measurements. Also, note that the downshift for the 1 layer model is less than that for the case with no ice layers. This occurs because truncation of the snow model has changed the thin layer configuration just above the snow-ground interface and slightly alters the spectrum of the reflected wave. This is also a factor in the 5 and 10 ice layer models, but is negligible relative to transmission attenuation.

[25] The 10 ice layer model yields a frequency shift of 85 MHz with W_{app} = 0.007. In this case, the apparent water content is approaching the level of uncertainty likely in field data and may therefore have a substantial impact on interpretation of results. It is important to note here that a thin layer of slush at the base of the snow pack can substantially alter the reflected spectrum, resulting in a shift to either higher or lower frequencies depending on thickness. For example, modeling shows that for a 0.05 m thick saturated slush layer at the snow base, the dominant frequency of the reflection can increase by as much as 28%. This effect will occur when substantial drainage is occurring through a very wet snowpack that overlies relatively impermeable material such as ice or bedrock. In such cases, the frequency-dependent attenuation measurement will be severely altered limiting the applicability of the method described here.

4. Field Examples

[26] We conducted two field studies to test the capabilities of GPR multifold and attenuation analysis for measuring snow density and SWE. The first was over a shallow (<1 m) dry winter snowpack on Freemont Pass, Colorado. The second data set was acquired over a moist spring snowpack near Lionhead Mountain, Montana.

4.1. Dry Snow Study: Freemont Pass, Colorado

[27] In this study we investigated a midwinter alpine snowpack in a flat open meadow at the summit of Freemont Pass (elevation 3450 m) near Leadville, Colorado. The work was conducted during a low-snowfall year with average snowpack in the area less than 60% of the 30 year annual average. The snow was less than 1 m deep and consisted almost entirely of faceted crystals with no shear strength. Temperatures on the day of acquisition and for at least several preceding weeks were well below freezing so the snow was cold and dry. Our primary objective was to test variability in the reference frequency and basal reflection frequency measurements under field conditions. In this case, we expected no downward shift in the signal spectrum.

4.1.1. Data Acquisition and Processing

[28] We acquired GPR data with a Sensors and Software PulseEkko 1000 system using 900 MHz antennas. The data consist of a 14.3 m long common-offset profile with 0.05 m trace spacing, and a CMP gather (expanding spread mode) with 0.05 m offset interval located near the center of the profile (Figure 5). The radar antennas were placed directly on the snow surface. For control, manual density measurements were made every 0.20 m vertically by using a 250 cm^3 snow sampler to collect and weigh a known volume sample in a snow pit located at the CMP position.

[29] Preprocessing for attenuation analysis included (1) time zero correction, (2) bandpass filter, and (3) an approximate spherical spreading correction by scaling the amplitude by t. We measured the velocity by picking the traveltime at the peak of the first sidelobe of the ground reflection. These traveltimes were then fit with the standard hyperbolic traveltime equation (normal-moveout) using a least squares routine yielding a velocity of 0.248 m/ns.

4.1.2. Results

[30] We computed the reference frequency in two ways. First, we measured the instantaneous frequency of the direct wave at every trace in the common offset gather. This method yielded a reference frequency of 712 ± 25 MHz with the given uncertainty being one standard deviation. It is important to recognize that the direct arrival in the common offset section is actually interference between the

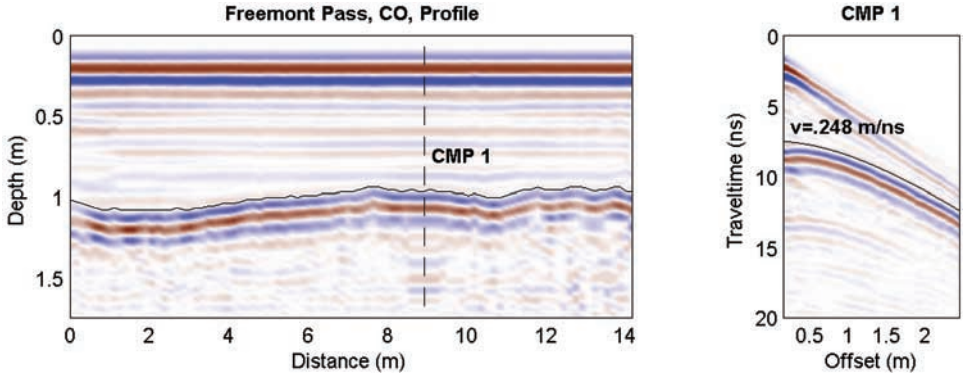

Figure 5. Common-offset profile and common-midpoint gather for the dry snow study conducted on Freemont Pass, Colorado. A snow pit was excavated at CMP where manual density measurements were acquired.

Table 2. Snow Properties Estimated From GPR and Rip Cutter Measurements at the Freemont Pass, Colorado Site[a]

Measurement	v (m/ns)	$f_0 - f_t$ (MHz)	Q^*	W	Snow Depth (m)	Snow Density (kg/m^3)	SWE (m)
GPR at CMP 1 (v, Q^*_s)	0.248	0.0	4	0.0	0.93	247	0.230
Manual density (snowpit)	NA	NA	NA	NA	0.95	245	0.233

[a]The quantity $f_0 - f_t$ is the change in dominant frequency between the direct wave through the snow and the snow/ground reflection.

direct air wave and direct snow wave and that this interference has the potential to alter the reference spectrum. Because of this potential problem, we also measured the frequency of the direct snow wave in the CMP gather at offsets from 0.10 m–1.00 m where the air wave is effectively separated from the direct snow wave. Note that with these shielded antennas, the direct air wave is very weak at all offsets. This method yielded a reference frequency of 712 ± 19 MHz. It is clear that the two methods are equivalent; the interfering air wave does not significantly alter the direct wave frequency measurement. In wet snow, we expect a frequency decrease with increasing offset so the CMP method would not be effective in this case.

[31] The peak frequency of the ground reflection, averaged over all traces was 733 ± 39 MHz, so that within measurement uncertainty there was no spectral shift indicating $W = 0$ as expected. Snow depth, density, and SWE were estimated at the CMP position from the GPR data (Table 2). The three GPR estimates are comparable to the manual measurements (Table 2) with SWE differing by only 1%. Uncertainties in the measured dominant frequencies were just 3.5% and 5.3% for the reference wave and ground reflection, respectively.

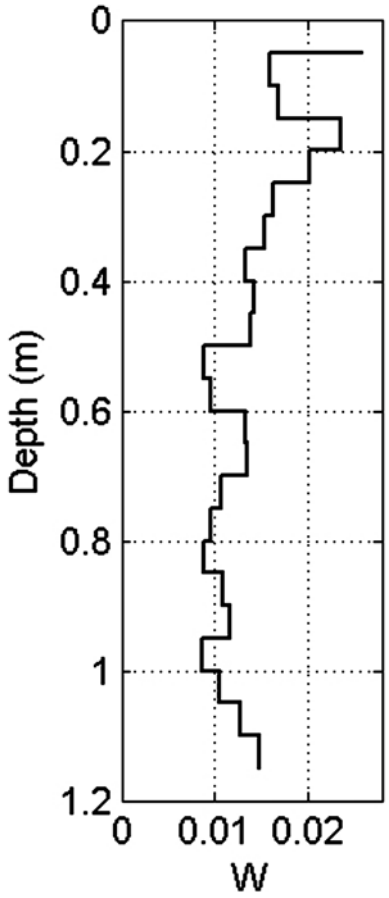

Figure 6. Wetness profile acquired at the Lionhead site using the Finnish Snow Fork. W is over 0.02 near the surface where melting is occurring but decreases with depth and has an average value of ~0.014.

4.2. Moist Snow Study: Lionhead, Montana

[32] For the moist snow case, we investigated an early spring snow pack near Lionhead Mountain, about 15 km west of West Yellowstone, Montana. The survey was conducted along a 35 m profile located within an open glade on a 25–30 degree northwest facing slope at 2350 m elevation. The depth of the snow measured in snowpits was ~1.2 m. The snowpack had experienced warm spring temperatures the week prior to field measurements with some surface melting. A cold clear night prior to our data collection froze the upper 0.05–0.10 m, which was thawing during data collection resulting in wetness reaching an average of ~0.014 (Figure 6). Air temperature at the start of acquisition was 8°C.

4.2.1. Data Acquisition and Processing

[33] We used a Sensors and Software PulseEKKO Pro GPR system with 1000 MHz antennas. We acquired the data with the GPR system suspended 0.70 m above the snow (Figure 7). This configuration enabled us to use the air/snow interface reflection for the reference waveform. This approach to measuring the reference spectrum is superior to making the measurement using the direct wave from a

Figure 7. Sled and operator in the configuration for acquiring multioffset GPR data with the 1000 MHz antennas suspended 0.70 m above the snow surface.

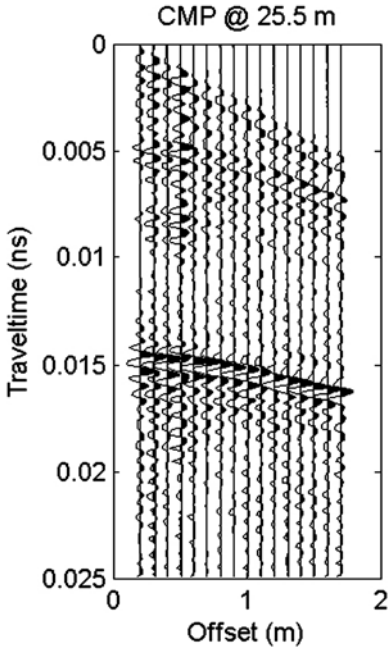

Figure 8. Common-midpoint gather from the moist snow study at Lionhead, Montana. The top of the snow reflection has a near offset arrival time of 5 ns, and the base of snow reflection arrives at 14 ns.

ground-coupled system because it eliminates direct wave interference and source/surface coupling. To attenuate noise in the reference frequency, we applied a running average filter to the instantaneous frequency over a 20 trace window then estimated uncertainty by computing the standard deviation over the same window. The same procedure was applied to the snow/ground reflection.

[34] To make laterally continuous measurements of radar propagation velocity in the snow, we acquired continuous multioffset data. The multioffset data were assembled by making 16 passes over the profile and increasing the source/receiver offset by 0.10 m on each pass giving an offset range from 0.20–1.70 m. The system was triggered approximately every 0.10 m using an odometer wheel. Snow build up on the odometer wheel resulted in minor trigger inconsistencies. We compensated for this problem by first assuming that the traces were uniformly distributed across the profile, then interpolating each common-offset profile onto a uniformly sampled profile with 0.10 m trace spacing. These positioning errors increased the uncertainty in our velocity measurements, but the interpolation procedure produced a set of common-midpoint gathers with few noticeable errors (Figure 8). Since the position errors were much smaller than the lateral scale over which the velocity measurements were made, we believe that the position errors did not significantly affect the results. Prior to velocity or attenuation analysis, we applied the same preprocessing steps as for the dry snow case above.

[35] To measure GPR propagation velocity in the snow pack, we used Stork's method of reflection tomography [*Stork*, 1992] in the prestack depth migration (PSDM) domain. This is an effective, robust analysis tool that can provide GPR velocity estimates with a resolution of 2–3 wavelengths at the dominant signal frequency and less than 2% uncertainty under typical field conditions [*Bradford et al.*, 2009]. The process of reflection tomography in the PSDM domain produces both a velocity model and a migrated reflection image in depth. PSDM improves the accuracy of the final reflection image by avoiding the assumptions of normal moveout analysis such as planar flat lying reflections and small velocity gradients [*Yilmaz*, 2001]. *Bradford* [2006, 2008] provided thorough reviews of this method as applied to GPR data processing and *Bradford et al.* [2009] gave a detailed description of applying Stork's method to groundwater aquifer characterization with GPR.

[36] Our instrumentation setup resulted in an air layer between the GPR antennas and snow surface (Figure 7). We constrained the tomographic inversion by holding the velocity of the air layer constant and equal to the speed of light (0.3 m/ns). We used a 0.10 m $\times$ 0.10 m cell size (equal to the trace spacing) to construct the tomographic velocity model and imposed a smoothing constraint with 5 m ($\sim$20 wavelengths) horizontal and 0.3 m ($\sim$1.2 wavelengths) vertical smoothing operators. We assume 2% uncertainty in the vertically averaged velocity model.

[37] Uncertainty in the three measured parameters (reference frequency, target frequency, and velocity) propagated through all subsequent calculations to produce uncertainty bounds in the resulting physical property estimates (ρ_d, W, and SWE).

[38] Control data were acquired in a snow pit located 20 m along the GPR profile and dug after GPR data acquisition. We used a Finnish Snow Fork [*Sihvola and Tiuri*, 1986] which computes real and imaginary dielectric permittivity using a 2 pronged waveguide that is inserted into the snow [*Tiuri et al.*, 1984]. Since the instrument measures the same electrical parameters that we measure with GPR, it provides an excellent tool for validating the GPR measurements and has been compared to radar measurements in previous studies [*Harper and Bradford*, 2003; *Marshall et al.*, 2005]. Wetness and dry snow density were estimated using equations (3)–(5). We acquired snow-fork measurements every 0.05 m vertically on the pit wall, and repeated the vertical profiles 3 times for a total of 72 snowfork measurements. For comparison to the GPR measurements, we computed bulk snow properties by averaging over each of the three vertical transects. The values we report here are the average and standard deviation of the three bulk values. In addition to the snow fork, we made measurements with the 250 cm^3 snow sampler and methods described in section 4.1.1.

4.2.2. Results

[39] The prestack depth-migrated image shows clear reflections from the top and base of the snowpack as well as a prominent internal reflection from an ice layer (Figure 9). The average velocity across the profile is 0.24 m/ns with one significant high-velocity zone between 10 and 20 m and a significant low-velocity zone between 20 and 27 m. A large bush (confirmed later by digging) lies between the high- and low-velocity zones and may have impacted deposition patterns leading to the anomalies.

[40] The mean reference frequency is 1347 MHz with a standard deviation of 3.5% along the profile. The mean frequency for the base of snow reflector is 1131 with a standard deviation of 9.6%. Greater variability in the basal reflection frequency is expected and reflects lateral changes

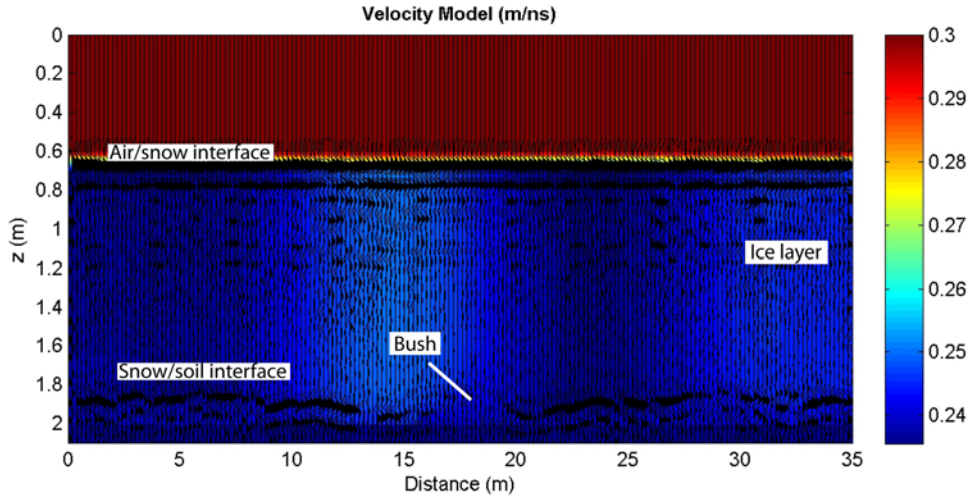

Figure 9. Velocity model from reflection tomography overlain by the prestack depth-migrated GPR image from the Lionhead study.

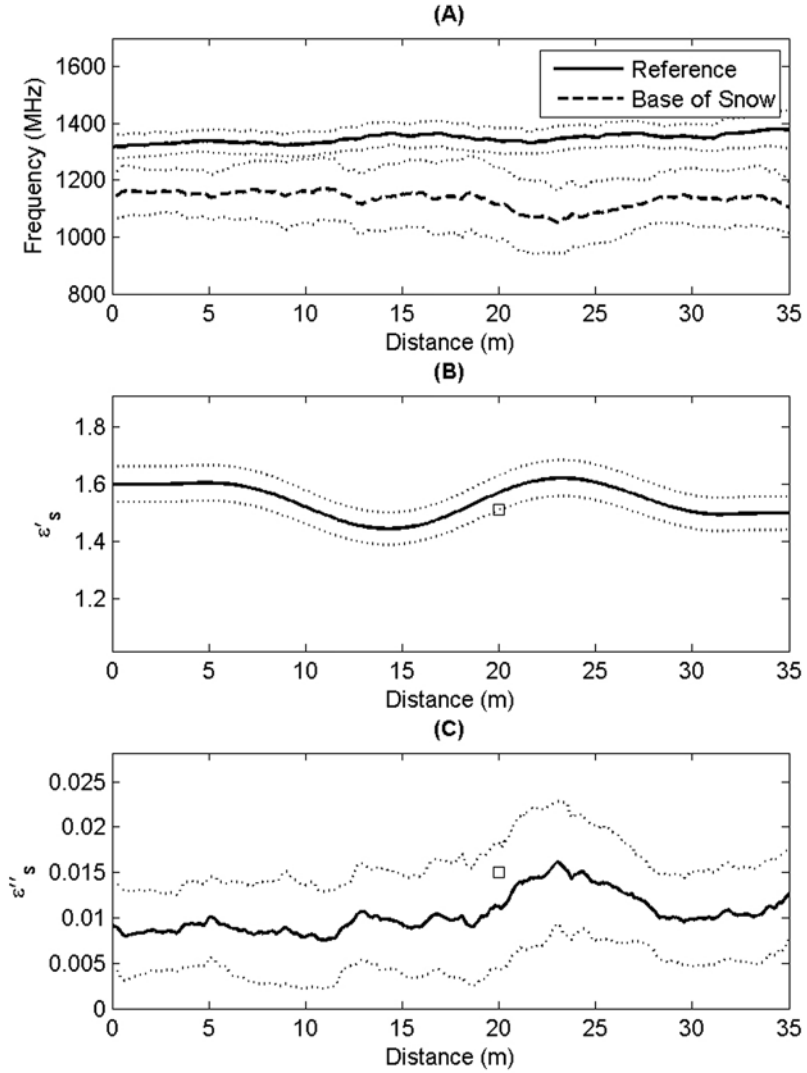

Figure 10. (a) Reference frequency from the snow surface reflection and target frequency from the base of snow reflection, (b) real relative permittivity, and (c) imaginary relative permittivity. In Figures 10b and 10c, snow fork average values for the bulk snowpack are shown with a square, and the symbol size is approximately twice the standard deviation. In all plots, uncertainty bounds for the GPR estimates are shown with dotted lines.

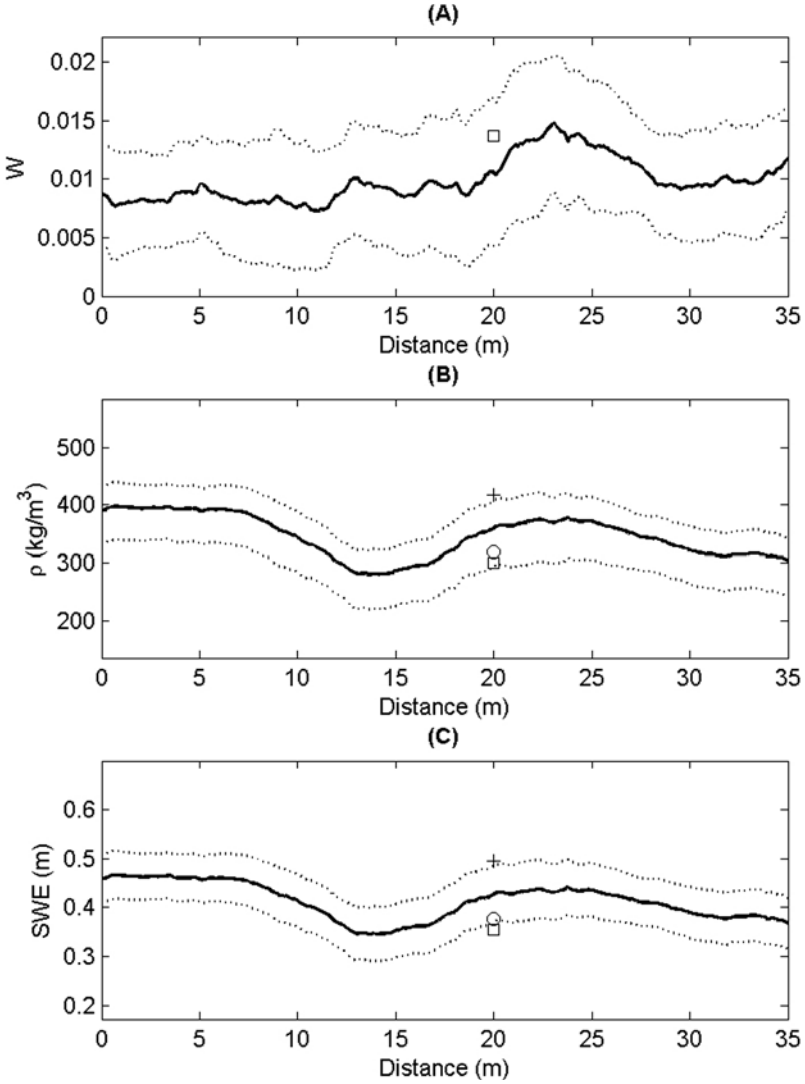

Figure 11. (a) Estimated wetness, (b) bulk snow density (snow + liquid water), and (c) SWE. GPR estimates are shown with a solid line, snow fork measurements are shown with a square, gravimetric measurements are shown with a circle, and the radar estimate assuming dry snow is shown with a plus. Uncertainty bounds for the GPR estimates are shown with dotted lines. The symbol size is approximately equal to twice the standard deviation in snow fork and gravimetric measurements.

in the snowpack as well as changes caused by heterogeneity at the snow-ground interface. The mean frequency downshift of 216 MHz is significant and lies outside of uncertainty bounds across the entire profile (Figure 10a). There is substantial lateral variability in the frequency downshift, most notably a greater shift is associated with the low-velocity zone between 20 and 27 m (Figure 10a).

[41] We converted the tomographic velocity profile to a profile of vertically averaged ε_s' (Figure 10b) then coupled this with the frequency downshift to estimate ε_s'' via equations (7) and (8) (Figure 10c). Note that variability in the measured frequencies is the primary contributor to the ε_s'' uncertainty. GPR electric permittivity estimates at 20 m along the profile ($\varepsilon_s' = 1.56 \pm 0.06$, $\varepsilon_s'' = 0.011 \pm 0.007$) are well within uncertainty bounds of the snow fork measurements ($\varepsilon_s' = 1.51 \pm 0.02$, $\varepsilon_s'' = 0.015 \pm 0.001$). Note that ε_s'' reported here are scaled to 1 GHz for comparison. The estimated water content from GPR ($W = 0.011 \pm 0.06$) is in good agreement with the snow fork measurements ($W = 0.014 \pm 0.001$) (Figure 11a). The GPR bulk density ($\rho_s = \rho_d + W\rho_w$) and SWE estimates ($\rho_s = 360 \pm 60$ kg/m^3, SWE = 0.42 ± 0.06 m), while still within uncertainty bounds, are somewhat higher than the snow fork measurement ($\rho_s = 300 \pm 1$ kg/m^3, SWE = 0.35 ± 0.01 m) and gravimetric measurements ($\rho = 320 \pm 2$ kg/m^3, SWE = 0.38 ± 0.03 m) (Figures 11b and 11c). The divergence in SWE and bulk density is primarily a function of the dry snow density estimate. For the snow fork calculation, a slightly lower ε_s' and slightly higher W both act to decrease the calculated density leading to greater divergence from the GPR estimated values than for other estimated parameters. Finally, we assumed dry snow ($\varepsilon_s'' = 0$) then computed apparent snow density and SWE ($\rho_{app} = 420$ kg/m^3, SWE$_{app}$ = 0.49 m). These values are 31% and 29% higher than the gravimetric values respectively, and demonstrate that even very small amounts of liquid water can substantially alter

the GPR estimated snow properties and must be taken into account.

5. Discussion

[42] SWE estimates based on calibration of the two-way traveltime assume laterally homogeneous snow or require interpolation between calibration points and may not accurately represent short-wavelength snow variability. Acquiring calibration data may be labor intensive and time consuming and therefore can substantially increase survey time and it is not practical, in large-scale surveys, to acquire sufficient calibration density to accurately represent short-wavelength lateral variability. This problem is particularly critical when liquid water is present in the snowpack since small variations of volumetric water distribution can substantially alter the dielectric permittivity and the assumption of lateral homogeneity can introduce significant error in the SWE estimates. Our new method enables laterally continuous measurement of liquid water content and snow density, and therefore directly accounts for short-wavelength lateral variability.

[43] An important point is the efficiency with which the required multioffset data can be acquired. In the two field examples presented in this study, we acquired GPR data with single channel GPR systems. In the case of the wet snow study, we acquired continuous multioffset data by repeating the survey 16 times with different transmitter-receiver offsets. Presently, all major GPR hardware vendors produce multichannel GPR systems that can dramatically increase the efficiency of acquiring multioffset data. For example, with an 8 channel system, utilizing 4 transmitters and 4 receivers, it is possible to simultaneously acquire 16 source-receiver offset pairs. *Bradford et al.* [2009] used such a system with a single transmitter and 4 receivers in the study of a shallow groundwater system. However, multichannel systems are expensive so optimizing the number of channels is an important consideration. As a test, we repeated the reflection tomography calculation for the wet snow study using only every fourth traces (a total of 4 source-receiver pairs). Comparing the velocity model computed from the sparse data with that computed with all 16 source-receiver offsets, we found that mean difference and standard deviation of the difference were less than 2% of the mean velocity. This is within the estimated uncertainty and therefore the difference is insignificant suggesting that 4 offsets are adequate to accurately represent the velocity field when distributed over an adequate offset range. Using reflection seismology as an analog, the rule of thumb is that the maximum offset should be equal to or greater than the depth of the snow and this condition was met for our studies. The 4 channel result should be taken with caution however since results will be site specific and depend on signal-to-noise and reflector complexity. We recommend 4 offsets at a minimum and as many as 16 or more if possible.

[44] Somewhat to our surprise, the numerical study indicates that fine layering will have a minor impact on spectral properties of the snow/soil reflection in most cases. However, the presence of several high-contrast layers (>5), such as ice layers, has the potential to alter the measurement and lead to incorrect results. Heterogeneity at the base of the snow pack that is at a scale less than the GPR dominant wavelength, such as a thin layer of slush, also has the potential to impact the spectral properties. Site-specific forward modeling, based on snow pit measurements, can help identify and compensate for potential problems. For the two examples given in this study, one ice layer was present in the wet snow study, and no buildup of water was present at the snow-ground interface so layering did not likely bias our results.

[45] The uncertainty of GPR estimated electric properties is substantially higher than that made using direct sampling methods or small-scale electrical instruments such as the snow fork. However, point measurements such as snow pit methods are not without inherent uncertainty related to issues such as support volume and can be difficult to interpolate because of local sampling of heterogeneity. The real strength of the GPR method is in providing bulk-averaged laterally continuous property measurements over large distances. As such, the GPR method is best implemented by integrating the GPR estimates with a limited number of direct measurements.

6. Conclusions

[46] Because the complex permittivity of snow is proportional to the complex permittivity of water, there is a simple functional form relating the slope of the GPR attenuation versus frequency curve to the complex dielectric permittivity. This calculation, along with velocity analysis to measure the real component of dielectric permittivity, enables detailed measurements of snow properties from surface GPR data including wetness, dry snow density, and SWE. The method proved to be sensitive and robust in our field studies. The frequency downshift method we utilize to characterize frequency-dependent attenuation depends on a robust measure of the dominant frequency of the GPR wavelet. For the data presented in this study, dominant frequency estimation based on instantaneous frequency analysis was stable with variability less than 5%. With this level of precision, we can make estimates of snow wetness with an absolute uncertainty of about 0.005 (water volume/total snow volume). The stability of the measurement is not surprising given the high signal-to-noise ratio typically associated with the air/snow and snow/soil reflectors Further, estimates of snow density and SWE agreed with snow fork and manual density measurements to within estimated uncertainty. While we considered only the pendular regime, it should be possible to extend the method to the funicular regime given appropriate petrophysical relationships.

[47] GPR can be deployed in either ground based or airborne modes and has the potential to provide laterally continuous estimates of SWE over large distances in either wet or dry snow. This capability is valuable as the need for careful water resource management becomes an increasingly important societal issue.

[48] **Acknowledgments.** We thank Karl Birkeland and Ron Johnson from the U.S. Forest Service National Avalanche Center for logistics support and Blaze Reardon for snowpit density measurements during the Lionhead experiment.

References

Bales, R. C., et al. (2006), Mountain hydrology of the western United States, *Water Resour. Res.*, *42*, W08432, doi:10.1029/2005WR004387.

Bradford, J. H. (2006), Applying reflection tomography in the post-migration domain to multi-fold GPR data, *Geophysics*, *71*(1), K1–K8.

Bradford, J. H. (2007), Frequency dependent attenuation analysis of ground-penetrating radar data, *Geophysics*, *72*, J7–J16.

Bradford, J. H. (2008), Measuring lateral and vertical heterogeneity in vadose zone water content using multi-fold GPR with reflection tomography, *Vadose Zone J.*, *7*, 184–193.

Bradford, J. H., and J. T. Harper (2005), Wavefield migration as a tool for estimating spatially continuous radar velocity and water content in glaciers, *Geophys. Res. Lett.*, *32*, L08502, doi:10.1029/2004GL021770.

Bradford, J. H., et al. (2009), Estimating porosity via ground-penetrating radar reflection tomography: A controlled 3D experiment at the Boise Hydrogeophysical Research Site, *Water Resour. Res.*, *45*, W00D26, doi:10.1029/2008WR006960.

Cayane, D. R. (1996), Interannual climate variability and snowpack in the western United States, *J. Clim.*, *9*, 928–948.

Denoth, A. (1980), The pendular-funicular liquid transition in snow, *J. Glaciol.*, *25*(91), 93–97.

Denoth, A. (2003), Structural phase changes of the liquid water component in Alpine snow, *Cold Reg. Sci. Technol.*, *37*, 227–232.

Elder, K., et al. (1991), Snow accumulation and distribution in an alpine watershed, *Water Resour. Res.*, *27*(7), 1541–1552.

Ellerbruch, D. A., and H. S. Boyne (1980), Snow stratigraphy and water equivalence measured with an active microwave system, *J. Glaciol.*, *26*(94), 225–233.

Fisher, E., et al. (1992), Acquisition and processing of wide-aperture ground-penetrating radar data, *Geophysics*, *57*, 495–504.

Greaves, R. J., et al. (1996), Velocity variation and water content estimated from multi-offset, ground-penetrating radar, *Geophysics*, *61*(3), 683–695.

Green, E., et al. (2004), *Snow, Weather, and Avalanches: Observational Guidelines for Avalanche Programs in the United States*, Am. Avalanche Assoc., Pagosa Springs, Colo.

Gubler, H., and M. Hiller (1984), The use of microwave FMCW radar in snow and avalanche research, *Cold Reg. Sci. Technol.*, *9*, 109–119.

Hamlet, A. F., et al. (2005), Effects of temperature and precipitation variability on snowpack trends in the western U.S., *J. Clim.*, *18*, 4545–4561.

Harper, J. T., and J. H. Bradford (2003), Snow stratigraphy over a uniform depositional surface: Spatial variability and measurement tools, *Cold Reg. Sci. Technol.*, *37*(3), 289–298.

Lundberg, A., and H. Thunehed (2000), Snow wetness influence on impulse radar snow surveys theoretical and laboratory study, *Nord. Hydrol.*, *31*(2), 89–106.

Marshall, H. P., et al. (2005), Estimating alpine snowpack properties using FMCW radar, *Ann. Glaciol.*, *40*(1), 157–162.

Morlet, J., et al. (1982), Wave propagation and sampling theory. Part I: Complex signal scattering in multilayered media, *Geophysics*, *47*(2), 203–221.

Muller, G. (1985), The reflectivity method: A tutorial, *J. Geophys.*, *58*, 153–174.

Olhoeft, G. R. (1981), Electrical properties of rocks, in *Physical Properties of Rocks and Minerals*, edited by Y. S. Touloukian et al., pp. 257–330, McGraw-Hill, New York.

Quan, Y., and J. M. Harris (1997), Seismic attenuation tomography using the frequency shift method, *Geophysics*, *62*(3), 895–905.

Robertson, J. D., and H. H. Nagomi (1984), Complex seismic trace analysis of thin beds, *Geophysics*, *49*, 344–352.

Serreze, M. C., et al. (1999), Characteristics of the western United States snowpack from snowpack telemetry (SNOTEL) data, *Water Resour. Res.*, *35*(7), 2145–2160.

Sihvola, A. H., and M. E. Tiuri (1986), Snow fork for field determination of the density and wetness profiles of a snow pack, *IEEE Trans. Geosci. Remote Sens.*, *GE-24*(5), 717–721.

Stewart, I. T., et al. (2004), Changes in snowmelt runoff timing in western North America under a "business as usual" climate change scenario, *Clim. Change*, *62*, 217–232.

Stork, C. (1992), Reflection tomography in the postmigrated domain, *Geophysics*, *57*(5), 680–692.

Tiuri, M. E., et al. (1984), The complex dielectric constant of snow at microwave frequencies, *IEEE J. Oceanic Eng.*, *OE-9*(5), 377–382.

Turner, G., and A. F. Siggins (1994), Constant Q attenuation of subsurface radar pulses, *Geophysics*, *59*, 1192–1200.

Yilmaz, O. (2001), *Seismic Data Analysis*, 2nd ed., 2027 pp., Soc. of Explor. Geophys., Tulsa, Okla.

J. H. Bradford and J. Brown, Center for Geophysical Investigation of the Shallow Subsurface MG-206, Boise State University, 1910 University Drive, Boise, ID 83725, USA. (johnb@cgiss.boisestate.edu)

J. T. Harper, Department of Geosciences, University of Montana, 32 Campus Drive #1296, Missoula, MT 59812, USA. (joel@mso.umt.edu)